The Impact of Supplemental Dropwindsonde Data on the Structure and Intensity of Tropical Storm Karen (2013) in the NCEP Global Forecast System

MICHAEL J. BRENNAN

NOAA/NWS/NCEP/National Hurricane Center, Miami, Florida

DARYL T. KLEIST* AND KATE HOWARD

NOAA/NWS/NCEP/Environmental Modeling Center, College Park, Maryland

SHARANYA J. MAJUMDAR

Rosenstiel School of Marine and Atmospheric Science, University of Miami, Miami, Florida

(Manuscript received 31 December 2014, in final form 10 March 2015)

ABSTRACT

The impact of assimilating synoptic surveillance dropwindsonde data on the analysis and forecast of the structure and intensity of Tropical Storm Karen (2013) was examined. Data-denial experiments were conducted using the NCEP hybrid 3D ensemble–variational GSI and forecasts were made using the NCEP GFS model. The assimilation of dropwindsonde data resulted in a slightly more tilted tropical cyclone vortex, stronger vertical wind shear, and more upper-tropospheric dry air west of Karen in the initial conditions. These differences grew with time in the GFS forecasts, and resulted in a weaker and more sheared vortex by 24 h in the forecast that included the dropwindsonde data. After 24 h, the cyclone reintensified in the experiment where dropwindsonde data were excluded, likely because of moist processes in a favorable region for synoptic-scale ascent ahead of a baroclinic trough. In contrast, the forecast including the dropwindsonde data kept Karen weak and also did a better job forecasting the structure and track of Karen. These results suggest that differences in the analysis and short-term evolution of Karen and the environment due to the dropwindsonde data played a role in the longer-term structure and intensity of the cyclone, including the distribution and magnitude of associated diabatic heating. These results strongly suggest that a systematic study be undertaken to examine the impact of these data on tropical cyclone structure and intensity, since previous work has focused largely on the impact on track.

1. Introduction

Previous work examining the impact of assimilating dropwindsonde data from NOAA's synoptic surveillance missions flown into tropical cyclones (TCs) has focused on the improvements to track forecasts in the NCEP GFS model (e.g., Aberson 2010; Majumdar et al. 2013). However, given improvements to the NCEP GSI (Wu et al. 2002) data assimilation scheme (Kleist et al. 2009; Wang et al. 2013) and increases in the horizontal resolution of the GFS model, the question arises as to whether these supplemental observations can also influence the GSI analysis and GFS forecasts of TC structure and intensity. The goal of this study is to investigate and quantify the impact of assimilating dropwindsonde data from one NOAA synoptic surveillance mission on the structure and intensity of Tropical Storm Karen (2013), a TC that posed several operational intensity prediction challenges.

Karen formed around 0600 UTC 3 October 2013 near the Yucatan Peninsula of Mexico with a maximum 1-min sustained wind speed of 45 knots [kt; $1\,\text{kt} = 0.51\,\text{m s}^{-1}$; Kimberlain (2014)]. Karen's intensity peaked at 55 kt later on 3 October, but the cyclone then steadily weakened in an environment of strong upper-level southwesterly flow north of an upper-level ridge on 4–5 October (not shown). Karen continued weakening and became a tropical depression with maximum winds of 30 kt south of Louisiana by 0000 UTC 6 October (Fig. 1a). The cyclone dissipated

* Current affiliation: Department of Atmospheric and Oceanic Science, University of Maryland, College Park, College Park, Maryland.

Corresponding author address: Dr. Michael J. Brennan, National Hurricane Center, 11691 SW 17th St., Miami, FL 33165.
E-mail: michael.j.brennan@noaa.gov

DOI: 10.1175/WAF-D-15-0002.1

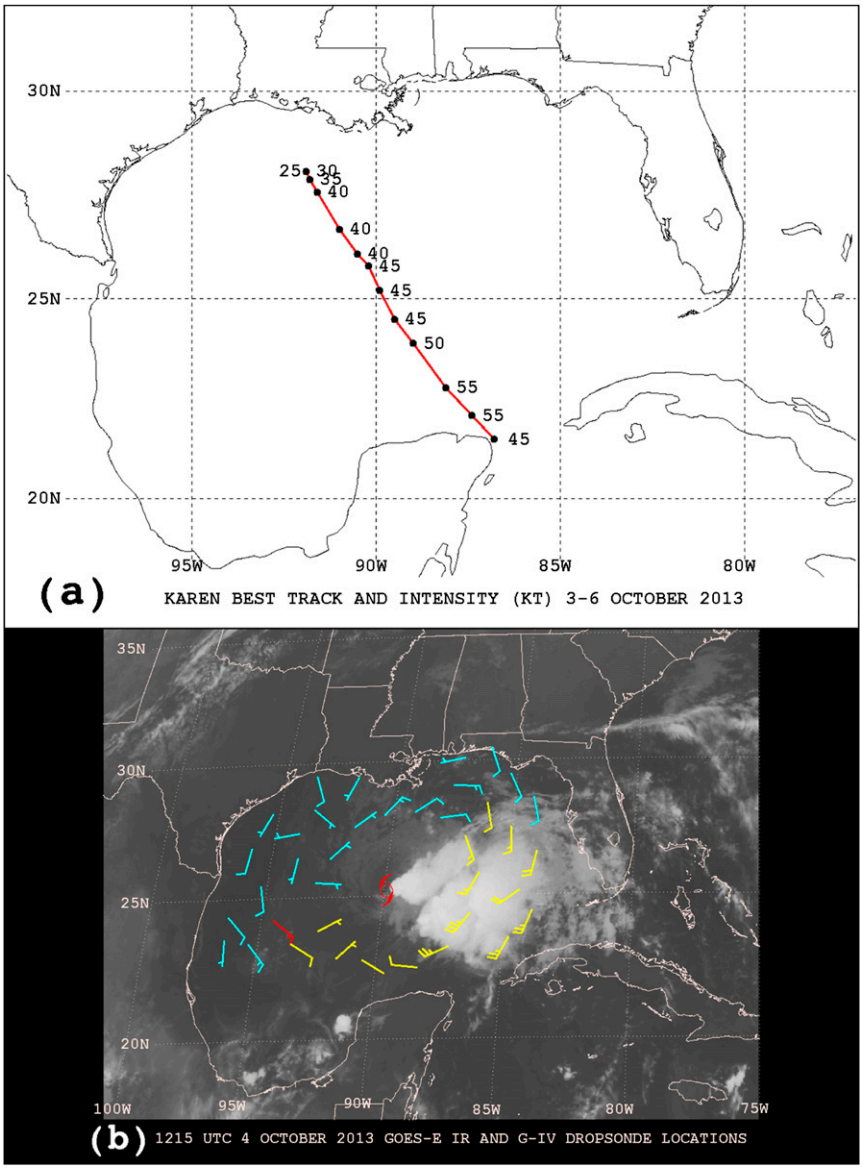

FIG. 1. (a) NHC final best track of Karen (red line) with 6-hourly positions indicated by black dots from 0600 UTC 3 Oct through 1200 UTC 6 Oct 2013 along with intensity (kt) shown beside each best-track point (note that the final two best-track positions are in the same location). (b) The 500-hPa wind barbs (kt) from NOAA G-IV synoptic surveillance mission dropwindsondes with 1145 UTC 4 Oct 2013 GOES-East infrared imagery. Yellow (cyan) wind barbs indicate dropwindsondes assimilated into the 0600 (1200) UTC 4 Oct GSI cycle. The red wind barb indicates a dropwindsonde that was not assimilated into either cycle. The tropical storm symbol indicates the center of Karen at 1200 UTC 4 Oct 2013.

around 1200 UTC 6 October south of the Louisiana coast, becoming one of only two TCs to form in the Gulf of Mexico and not make landfall during the aircraft reconnaissance era (Kimberlain 2014). By 0000 UTC 7 October, the circulation of Karen had dissipated and the remnant low-level trough was moving eastward ahead of an approaching mid-/upper-level trough moving into the Mississippi River valley (not shown).

Despite the relatively unfavorable environment for intensification, intensity guidance and the official NHC forecasts early in Karen's life showed the cyclone intensifying to near hurricane strength as it approached the northern coast of the Gulf of Mexico. These forecasts prompted the issuance of a hurricane watch from Grand Isle, Louisiana, to Indian Pass, Florida, at 1300 UTC 3 October (Kimberlain 2014).

Since Karen posed a possible hurricane threat to the United States, a synoptic surveillance mission was deployed around Karen on 4 October using the NOAA Gulfstream-IV (G-IV) jet. The mission consisted of 38 dropwindsondes released over the central and northern Gulf of Mexico around Karen (Fig. 1b).

During the event in an operational forecast setting, the first author noted a significant change in the forecast structure and intensity of Karen in the 1200 UTC 4 October GFS forecast: "in particular the GFS is weaker with its forecast of Karen after data from the NOAA Gulfstream-IV jet [...] which showed 200-mb winds west of Karen stronger than previously analyzed [...] were incorporated into the 12Z analysis." (Brennan 2013). The hurricane watch for the Gulf Coast was discontinued at 2100 UTC 4 October, in part because of the changes in the GFS model forecast (Brennan 2013).

In section 2, the data assimilation scheme and data-denial methodology employed in the operational GSI–GFS is presented, followed by results in section 3. The paper concludes with a summary and discussion of potential future work.

2. Methodology

The G-IV synoptic surveillance mission on 4 October deployed 38 dropwindsondes over the Gulf of Mexico around Karen. Fifteen of the dropwindsondes, mainly to the south and east of Karen, were available for the 0600 UTC cycle, while 22 others were available for the 1200 UTC cycle[1] (Fig. 1b).

At the time of Karen, the operational GSI–GFS had a horizontal spectral resolution of T574, equivalent to a horizontal grid spacing of approximately 27 km, and 64 vertical levels.[2] The data assimilation system utilized the GSI-based hybrid 3D ensemble–variational algorithm (EnVar; Lorenc 2013), where the background error covariance is constructed as a linear combination of a static climatological estimate (25%) with that prescribed by an 80-member ensemble (75%). The ensemble had a horizontal spectral resolution of T254 with the same number of vertical levels and was updated using the serial square root ensemble Kalman filter (EnKF) of Whitaker and Hamill (2002). More details regarding the hybrid configuration can be found in Kleist (2012), Wang et al. (2013), and Kleist and Ide (2015). Hamill et al. (2011) demonstrated that the use of a hybrid assimilation algorithm resulted in reduced deterministic TC track errors for the NCEP GFS. In addition to EnVar, the operational initialization of TCs in the GSI–GFS utilized both vortex relocation and the assimilation of the NHC operational synoptic time minimum sea level pressure estimates as an observation (Kleist 2011).

The data-denial methodology comprises two parallel assimilation–forecast cycles in the GSI–GFS.[3] The cycled control experiment (CTRL), which closely replicates the operational cycle, was begun at 0000 UTC 4 October and continued through 0000 UTC 7 October. The CTRL experiment assimilated the dropwindsonde data together with all observational data available for assimilation into the operational GSI–GFS. The operationally available observations include radiosonde, surface, aircraft, satellite-derived atmospheric motion vectors, wind profiler, ship and buoy, scatterometer-based surface winds, satellite microwave and infrared radiances, and satellite-based global positioning system radio occultation. The data-denial experiment (NODROP) was begun from the same initial conditions as CTRL at 0000 UTC 4 October. The observational data available for NODROP were identical to CTRL except for the exclusion of all G-IV dropwindsonde data during the 0600 and 1200 UTC 4 October cycles. The exclusion involved reprocessing the observation file each cycle, prior to the analysis being performed, to flag the specific G-IV dropwindsonde data for denial. Both experiments were fully cycled with a 6-h update frequency (including early and late cycles) and a 6-h assimilation window (±3 h), as in NCEP operations, for the entire experiment period. All observations that arrived by T + 0245 (T + 0545) for a given window were assimilated into that early (late) cycle. More details regarding the operational data assimilation cycling can be found in Kleist et al. (2009).

3. Results

We will examine the differences between the CTRL and NODROP analyses from the 1200 UTC 4 October cycle, since this comparison allows for the assessment of the impact of the 37 G-IV dropwindsondes that were assimilated into the GFS. The structure of the 925–700-hPa potential vorticity (PV) maxima is similar in the CTRL and NODROP analyses (Fig. 2). On the other hand, there is stronger 850–200-hPa vertical wind shear in CTRL, with a broader area containing values above 40 kt. An

[1] Drop 16, located at 23.9°N, 94.0°W, was received too late to be incorporated into the 0600 UTC cycle and too early to be incorporated into the 1200 UTC cycle.

[2] The experiments performed here used a configuration of the GSI–GFS that was as close as possible to the operational versions of the code at the time the experiments were performed.

[3] Note that both the CTRL and NODROP experiments were performed on NCEP's Zeus research and development supercomputer to avoid the complication of any computational differences when comparing the results of the experiments.

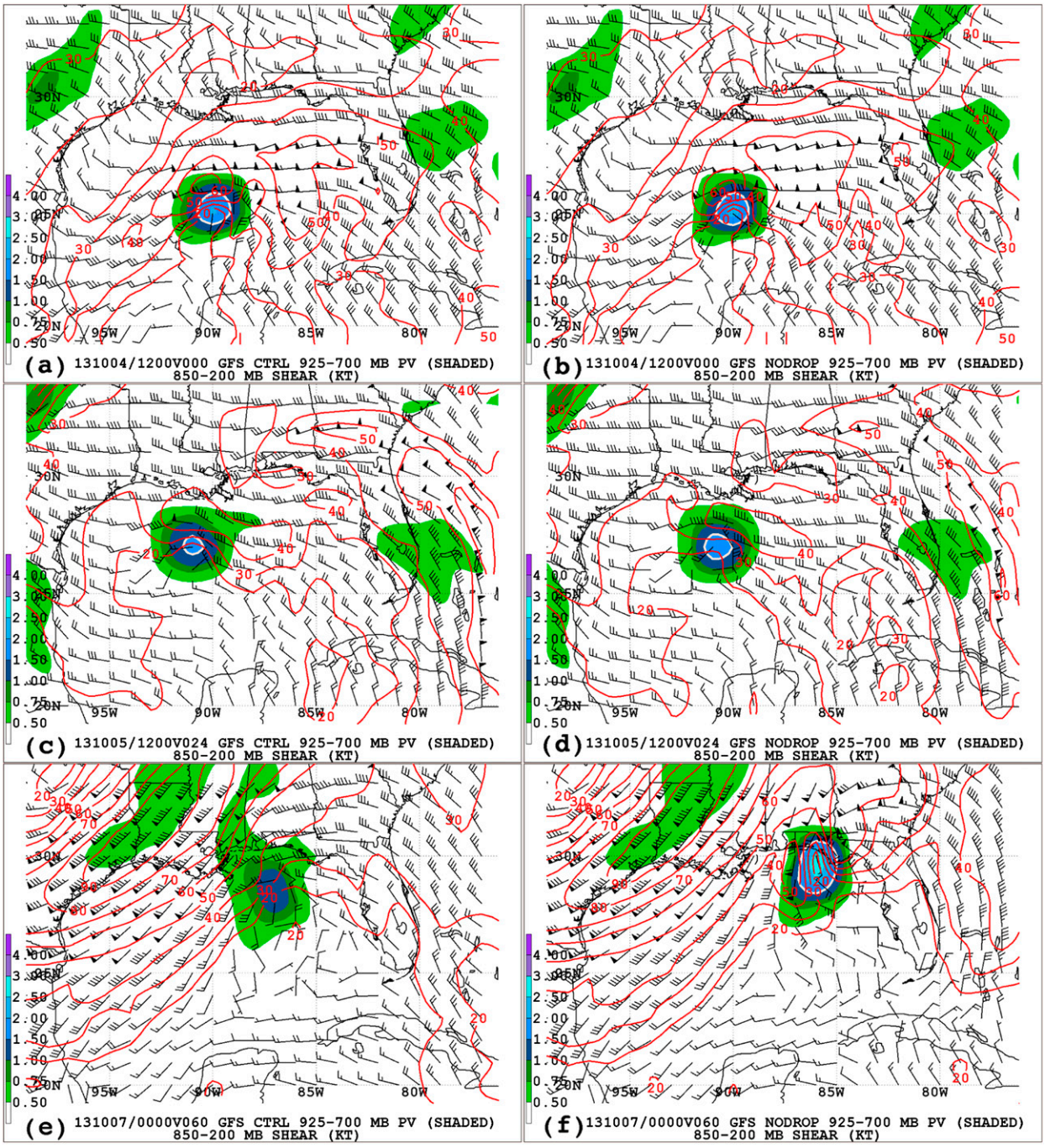

FIG. 2. (a) CTRL experiment analysis of 925–700-hPa PV (PVU; shaded with 1.5-PVU contour highlighted in white), 850–200-hPa wind shear (kt; barbs), and shear magnitude (kt; red contours every 10 kt beginning at 20 kt) valid at 1200 UTC 4 Oct 2013. (b) As in (a), but for NODROP. (c) As in (a), but for the 24-h forecast valid at 1200 UTC 5 Oct 2013. (d) As in (c), but for NODROP. (e) As in (a), but for the 60-h forecast valid at 0000 UTC 7 Oct 2013. (f) As in (e), but for NODROP.

examination of a west–east cross section through the vortex reveals that the CTRL analysis (Fig. 3a) shows a more tilted PV tower through the 500-hPa level than does the NODROP analysis (Fig. 3b). The horizontal separation between the 850- and 500-hPa vorticity maxima is about 55 nautical miles (n mi; 1 n mi = 1.852 km) in CTRL compared to 40 n mi in NODROP (not shown). In addition, CTRL shows drier air at 300 hPa and above over the vortex compared to NODROP. Finally, winds above the 250-hPa level were stronger in CTRL to the west of

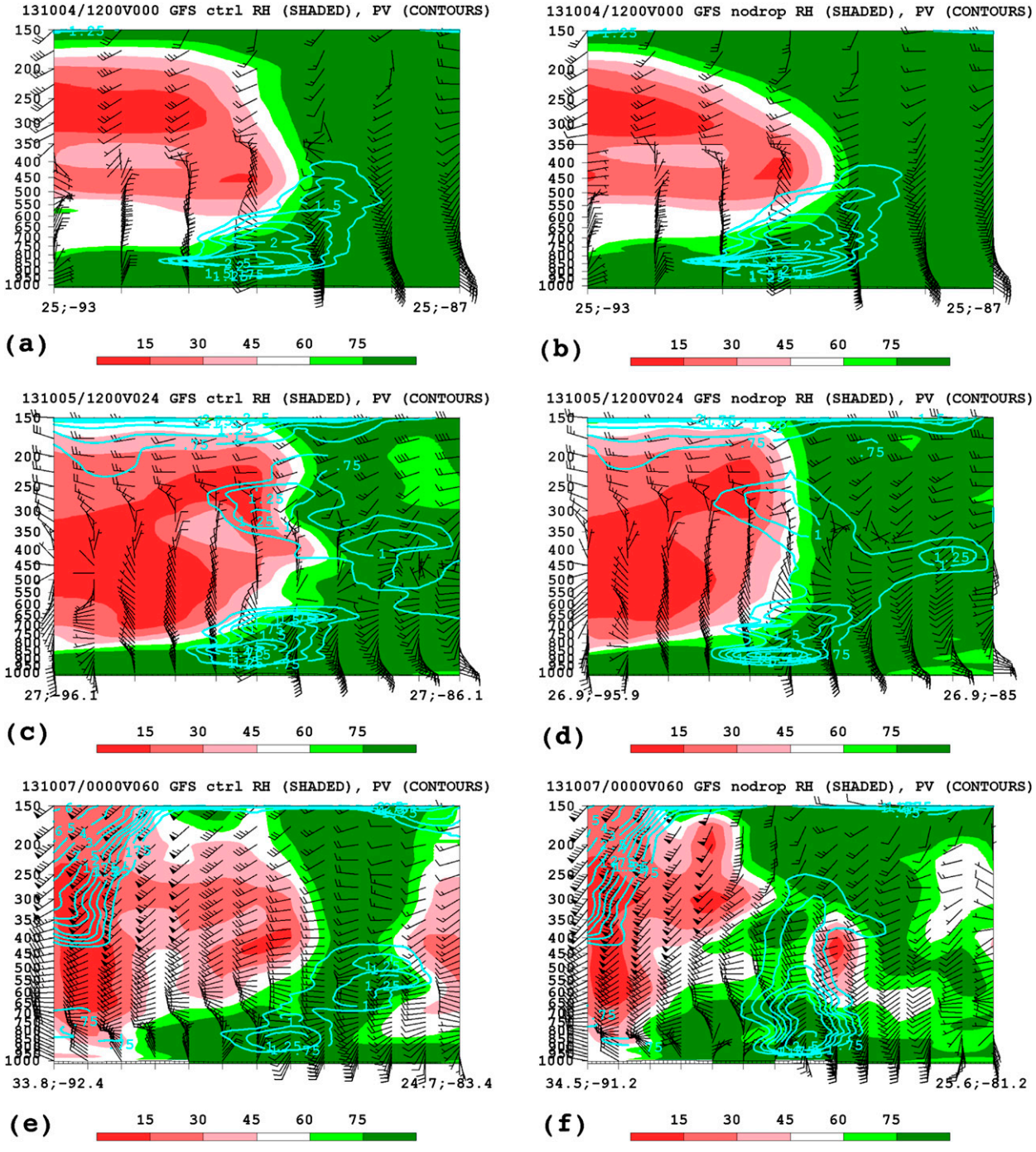

FIG. 3. (a) CTRL-analyzed cross section of relative humidity (shaded), PV (PVU; cyan contours starting at 1.25 PVU), and wind (kt; barbs) from 25.0°N, 93.0°W to 25.0°N, 87.0°W valid at 1200 UTC 4 Oct 2013. (b) As in (a), but for NODROP. (c) As in (a), but for the 24-h forecast valid at 1200 UTC 5 Oct 2013 from 27.0°N, 96.1°W to 27.0°N, 86.1°W and PV contours starting at 0.75 PVU. (d) As in (c), but for NODROP from 26.9°N, 95.9°W to 26.9°N, 85.0°W. (e) As in (c), but for the 60-h forecast valid at 0000 UTC 7 Oct 2013 from 33.8°N, 92.4°W to 24.7°N, 83.4°W. (f) As in (e), but for NODROP from 34.5°N, 91.2°W to 25.6°N, 81.2°W.

Karen, consistent with the higher vertical shear seen in the GFS analysis at the time (not shown).

To examine the correction of the vertical structure in the CTRL analysis due to the assimilation of the dropwindsonde data, soundings are drawn from the CTRL and NODROP analyses and compared against those from the dropwindsondes (which are not independent data in the CTRL analyses). As an example, a dropwindsonde

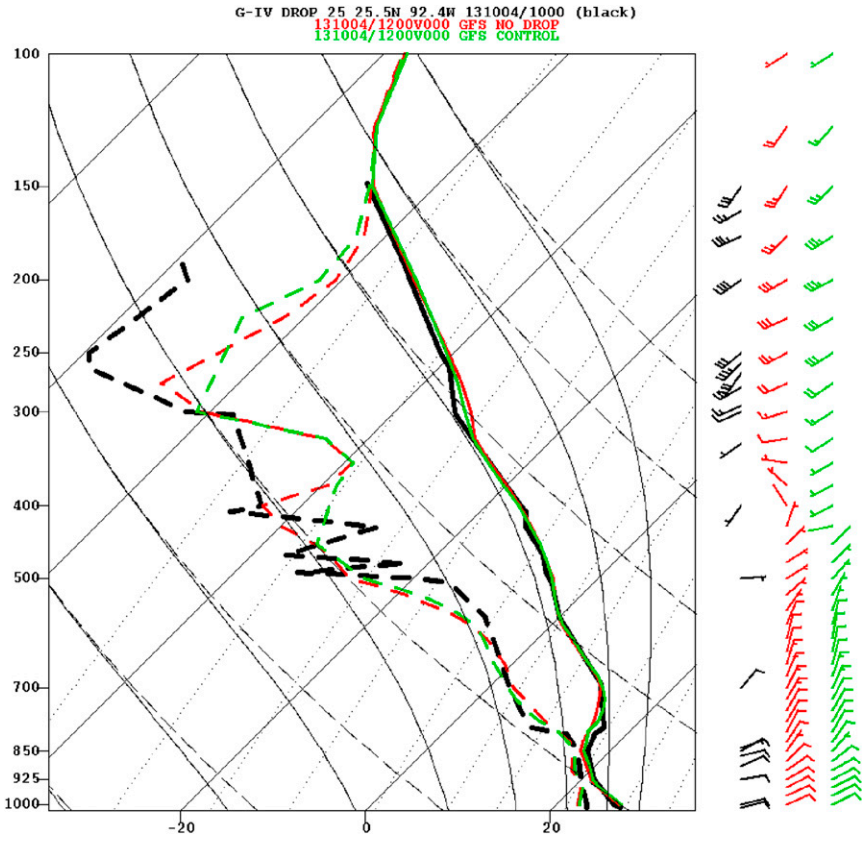

FIG. 4. Skew-temperature diagram of dropwindsonde 25 at 25.5°N, 92.4°W around 1000 UTC 4 Oct 2013 (black), compared with GFS NODROP (red) and CTRL (green) analyses at the same location valid at 1200 UTC 4 Oct 2013. Temperature (dewpoint) profiles (°C) are shown by solid (dashed) lines and wind (kt) is given by barbs.

released at 25.0°N, 92.4°W (west of Karen), at 1000 UTC measured winds of 30–40 kt between 250 and 175 hPa (Fig. 4). The corresponding 1200 UTC CTRL wind speeds around 200 hPa are accordingly corrected to be 5–10 kt stronger than those in the equivalent NODROP analysis.

For the 24-h forecasts valid at 1200 UTC 5 October, the differences between CTRL and NODROP increase. The lower-tropospheric PV maximum in CTRL is weaker than in NODROP, with a smaller region where the PV exceeds 1.5 potential vorticity units (PVU; 1 PVU = $10^{-6}\,\mathrm{K\,kg^{-1}\,m^2\,s^{-1}}$) and a larger area of 30–40 kt of vertical wind shear north of Karen (Figs. 2c,d). A comparison between the respective vertical cross sections shows even more pronounced differences. The Karen vortex in CTRL (Fig. 3c) shows an increase in tilt compared with the initial time 24 h earlier and is completely decoupled from the midtropospheric PV maximum located to the east. Also, CTRL shows drier air with relative humidity values less than 50% situated over much of the Karen vortex above the 500-hPa level. In NODROP (Fig. 3d), the dry air is displaced farther west and the vortex is less tilted. The horizontal separation between the 850- and 500-hPa vorticity maxima in CTRL is about 270 n mi compared with about 150 n mi in NODROP (not shown).

Moving ahead to the 60-h forecasts valid at 0000 UTC 7 October, the low-level Karen vortex remains weak in CTRL, with PV values less than 1.5 PVU, and moderate-to-strong deep-layer shear occurring over and northwest of the vortex center (Fig. 2e). In contrast, the NODROP forecast shows a vortex that has reintensified, with lower-tropospheric PV exceeding 2.5 PVU, despite the presence of strong shear (Fig. 2f).[4] The vertical structure of the Karen vortex is also quite different in the experiments. The CTRL cross section continues to show a shallow tilted vortex with dry air in the mid- and upper troposphere situated over the center of the low-level vortex (Fig. 3e). However, NODROP shows a vertically aligned Karen vortex that extends into the mid- and upper troposphere embedded in a moister environment (Fig. 3f).

[4] Note that some of the increase in shear seen in NODROP is due to the strengthening of the low-level flow around the vortex itself.

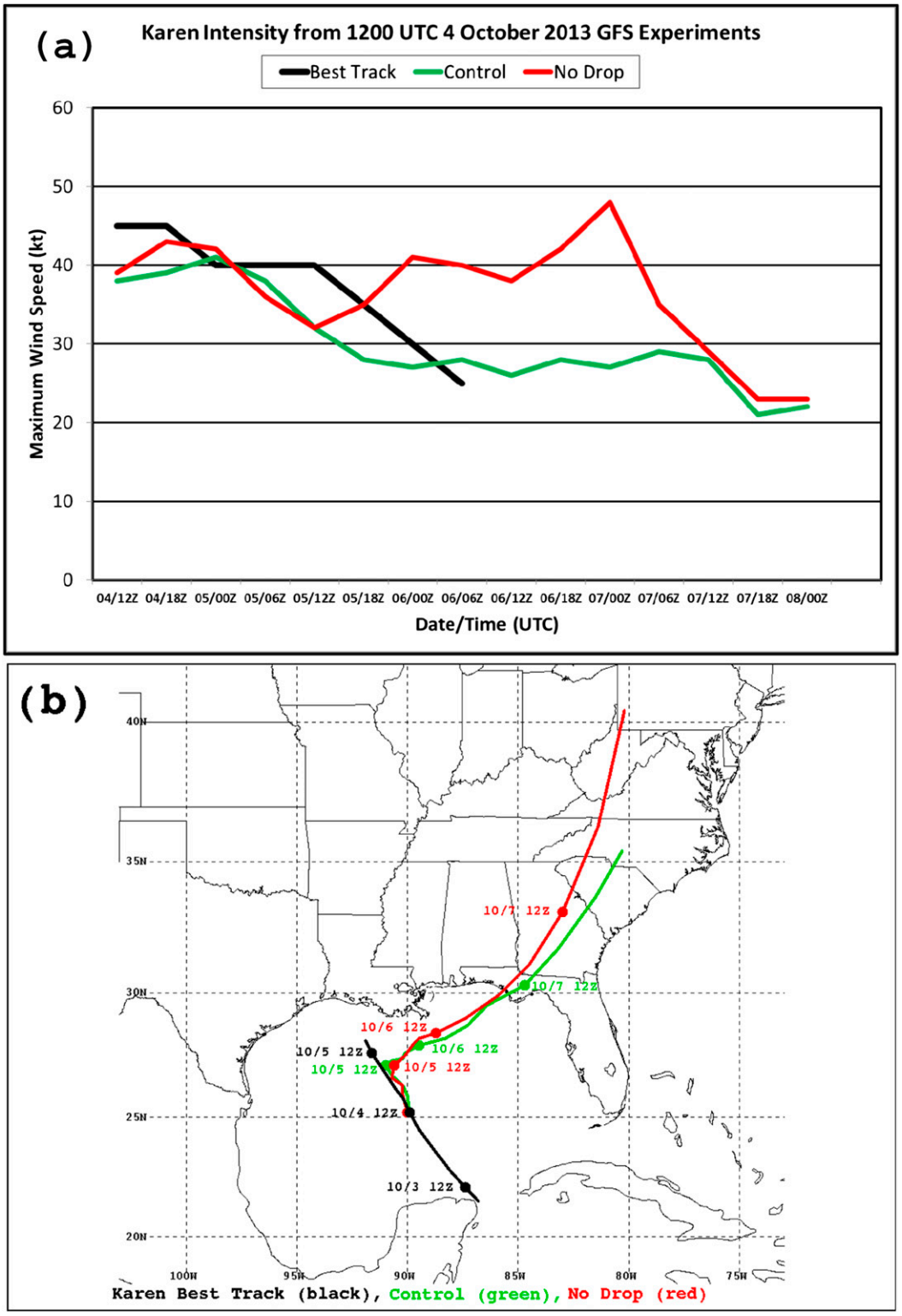

FIG. 5. (a) Time series of max winds (kt) in Karen from the 1200 UTC 4 Oct CTRL (green) and NODROP (red) GFS experiments with the NHC best track (black). (b) Track of Karen from the 1200 UTC 4 Oct CTRL (green) and NODROP (red) GFS runs with the NHC best track (black). Black dots indicate the best-track positions at 1200 UTC 3–5 Oct 2013. Red and green dots show the forecast positions of Karen at 1200 UTC each day starting on 5 Oct 2013 from NODROP and CTRL, respectively.

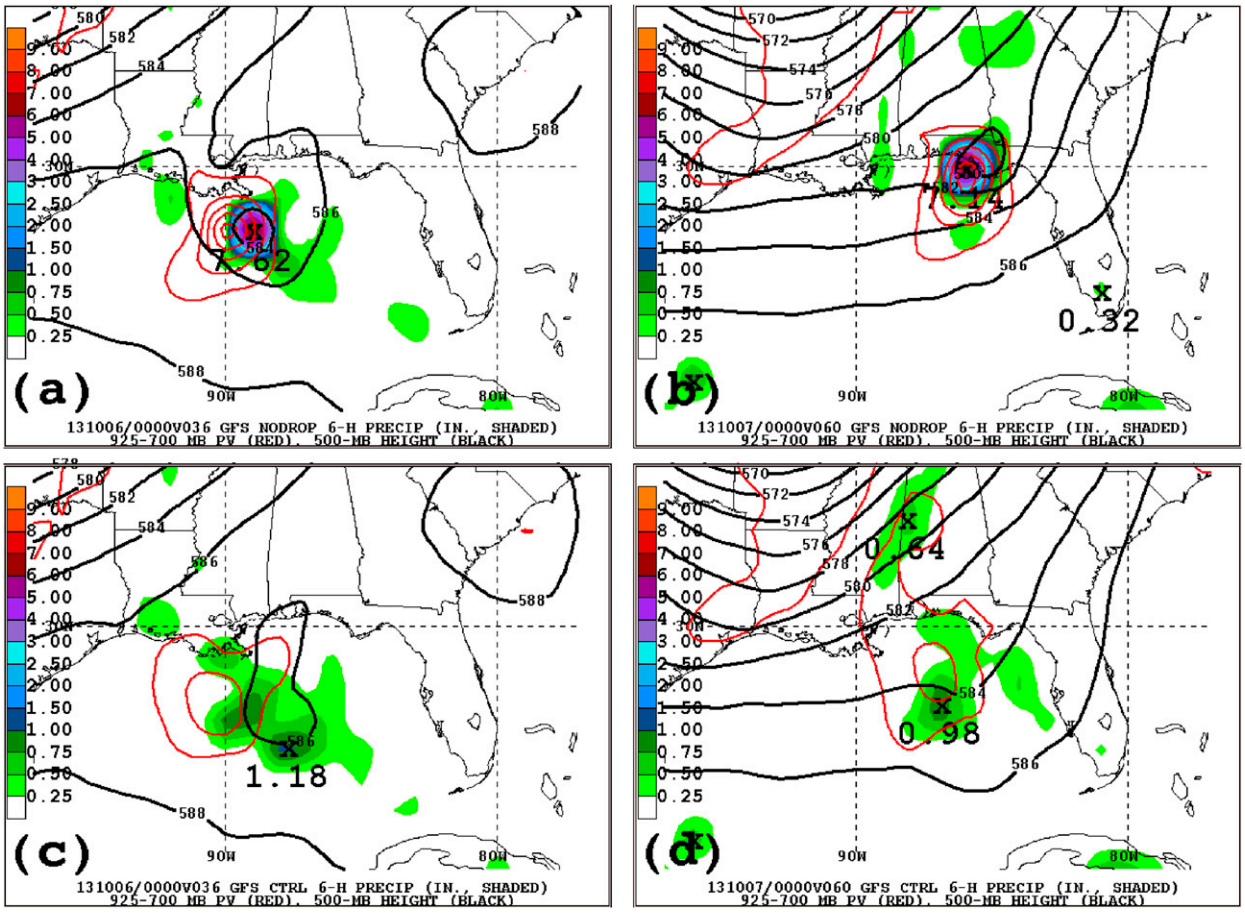

FIG. 6. (a) NODROP 6-h precipitation ending at 0000 UTC 6 Oct 2013 (in.; shaded), 925–700-hPa PV (PVU; red contours every 0.5 PVU starting at 0.5 PVU), 500-hPa geopotential height (dam; black contours every 2 dam). (b) As in (a), but for the period ending at 0000 UTC 7 Oct 2013. (c) As in (a), but for CTRL. (d) As in (b), but for CTRL.

A time series of maximum surface winds from NODROP and CTRL (Fig. 5a) shows that the reintensification of NODROP begins after 1200 UTC 5 October. The NODROP vortex reaches 40 kt around 0000 UTC 6 October and then strengthens to near 50 kt by 0000 UTC 7 October. In contrast, the CTRL vortex remains steady state between 25 and 30 kt from 1200 UTC 5 October through 1200 UTC 7 October. The track of Karen is also quite different, as NODROP shows a much faster northeastward acceleration ahead of the approaching upper-level trough, consistent with the deeper vortex in that experiment relative to the shallower CTRL vortex (Fig. 5b).

While a comprehensive diagnosis of the reintensification of the vortex in NODROP is beyond the scope of this study, an examination of the model fields suggests that it was likely driven in part by moist processes. NODROP 6-hourly precipitation totals near the vortex ending at 0000 UTC 6 October (Fig. 6a) and 0000 UTC 7 October (Fig. 6b) exceeded 7 in. (178 mm), while in CTRL the precipitation totals during the same periods (Figs. 6c,d) were around 1 in. (25 mm). This heavy precipitation in NODROP would be consistent with intensification of the lower-tropospheric vortex via diabatic processes in a favorable baroclinic environment, and is consistent with the timing of the strengthening seen in NODROP (Fig. 5a). These large differences in the precipitation evolution between CTRL and NODROP suggest that the intensity of the Karen vortex could be quite sensitive to differences in moisture, vertical shear, and how precipitation near the vortex evolves in response to large-scale baroclinic forcing for ascent ahead of the upper trough advancing through the southern United States.

4. Summary and conclusions

The impact of assimilating NOAA G-IV synoptic surveillance dropwindsonde data on the analysis and forecasts of Tropical Storm Karen (2013) in the NCEP

GSI–GFS system has been examined. Results from two parallel-cycled data assimilation experiments, CTRL, which assimilates all data used operationally, and NODROP, which withholds the G-IV data, indicate that the G-IV data contributed to a slightly more tilted vortex, stronger vertical wind shear, and drier air in the upper troposphere in the GSI analysis at 1200 UTC 4 October. These differences in structure increased during the GFS model forecasts, and by 24 h resulted in a weaker and more tilted vortex in CTRL relative to NODROP.

Beyond that time, the vortex in NODROP began to intensify, likely as a result of moist processes, which resulted in a much more vertically coherent vortex by 0000 UTC 7 October relative to CTRL. This suggests that differences in the analysis and short-term evolution of the Karen vortex and the environment due to the G-IV dropwindsonde data played a role in the longer-term evolution of the structure and intensity of the cyclone, including the distribution and magnitude of diabatic heating associated with Karen. In particular, the vortex in CTRL did not intensify, despite being located within a similar large-scale regime of forcing for ascent in the equatorward entrance region of an upper-level jet as the vortex in NODROP. These longer-range differences in the structure and intensity of the cyclone also contributed to longer-range differences in the track of the system.

Since these results are only from a single case, it is not possible to draw any broad conclusions about the impact of these supplemental data on TC structure and intensity within the GSI–GFS system. However, these results strongly suggest that a more systematic study using additional cases should be undertaken to examine the impact of these data on TC structure and intensity, since previous work has focused largely on the impact of these observations on TC track. One focus of future work should be on developing a more sophisticated methodology for targeting the spatial and temporal distribution of the supplemental data, given the implementation of a more sophisticated data assimilation system at NCEP, planned increases in the resolution of the NCEP global model, and the potential to improve the analysis and short-term forecasts of TC structure and intensity. Additional future work could include performing an ensemble forecast sensitivity to observations (EFSO) study to complement the data-denial results here and the investigation of the use of ensemble sensitivities derived from the EnKF-based ensemble for targeting.

Acknowledgments. We would like to gratefully acknowledge the efforts of the Gulfstream-IV crew from the NOAA Aircraft Operations Center who collected the dropwindsonde data used in this study. We would also like to thank two anonymous reviewers, Drs. Chris Landsea and Richard Pasch of NHC, and Dr. Vijay Tallapragada of EMC, who all provided helpful comments on previous versions of this manuscript.

REFERENCES

Aberson, S. D., 2010: 10 years of hurricane synoptic surveillance (1997–2006). *Mon. Wea. Rev.,* **138,** 1536–1549, doi:10.1175/2009MWR3090.1.

Brennan, M. J., 2013: Tropical Storm Karen discussion number 7. National Hurricane Center, accessed 1 May 2014. [Available online at http://www.nhc.noaa.gov/archive/2013/al12/al122013.discus.007.shtml.]

Hamill, T. M., J. S. Whitaker, D. T. Kleist, M. Fiorino, and S. G. Benjamin, 2011: Predictions of 2010's tropical cyclones using the GFS and ensemble-based data assimilation methods. *Mon. Wea. Rev.,* **139,** 3243–3247, doi:10.1175/MWR-D-11-00079.1.

Kimberlain, T., 2014: Tropical Storm Karen (AL 122013). National Hurricane Center Tropical Cyclone Rep., 15 pp. [Available online at http://www.nhc.noaa.gov/data/tcr/AL122013_Karen.pdf.]

Kleist, D. T., 2011: Assimilation of tropical cyclone advisory minimum sea level pressure in the NCEP Global Data Assimilation System. *Wea. Forecasting,* **26,** 1085–1091, doi:10.1175/WAF-D-11-00045.1.

——, 2012: An evaluation of hybrid variational–ensemble data assimilation for the NCEP GFS. Ph.D. thesis, University of Maryland, College Park, 149 pp. [Available online at http://drum.lib.umd.edu/handle/1903/13135.]

——, and K. Ide, 2015: An OSSE-based evaluation of hybrid variational–ensemble data assimilation for the NCEP GFS, Part I: System description and 3D-hybrid results. *Mon. Wea. Rev.,* **143,** 433–451, doi:10.1175/MWR-D-13-00351.1.

——, D. F. Parrish, J. C. Derber, R. Treadon, W.-S. Wu, and S. J. Lord, 2009: Introduction of the GSI into the NCEP Global Data Assimilation System. *Wea. Forecasting,* **24,** 1691–1705, doi:10.1175/2009WAF2222201.1.

Lorenc, A. C., 2013: Recommended nomenclature for EnVar data assimilation methods. Research Activities in Atmospheric and Oceanic Modeling, WGNE, 2pp. [Available online at http://www.wcrp-climate.org/WGNE/BlueBook/2013/individual-articles/01_Lorenc_Andrew_EnVar_nomenclature.pdf.]

Majumdar, S. J., M. J. Brennan, and K. Howard, 2013: The impact of dropwindsonde and supplemental rawinsonde observations on track forecasts for Hurricane Irene (2011). *Wea. Forecasting,* **28,** 1385–1403, doi:10.1175/WAF-D-13-00018.1.

Wang, X., D. Parrish, D. Kleist, and J. Whitaker, 2013: GSI 3DVar-based ensemble–variational hybrid data assimilation for NCEP Global Forecast System: Single-resolution experiments. *Mon. Wea. Rev.,* **141,** 4098–4117, doi:10.1175/MWR-D-12-00141.1.

Whitaker, J. S., and T. M. Hamill, 2002: Ensemble data assimilation without perturbed observations. *Mon. Wea. Rev.,* **130,** 1913–1924, doi:10.1175/1520-0493(2002)130<1913:EDAWPO>2.0.CO;2.

Wu, W.-S., D. F. Parrish, and R. J. Purser, 2002: Three-dimensional variational analysis with spatially inhomogeneous covariances. *Mon. Wea. Rev.,* **130,** 2905–2916, doi:10.1175/1520-0493(2002)130<2905:TDVAWS>2.0.CO;2.